Five-year (2004-2009) Observations of Upper Tropospheric Water Vapor and Cloud Ice from MLS and Comparisons with GEOS-5 analyses

Jonathan H. Jiang[1], Hui Su[1], Steven Pawson[2], Hui-Chun Liu[2], William Read[1], Joe W. Waters[1], Michelle Santee[1], Dong L. Wu[1], Michael Schwartz[1], Alyn Lambert[1], Ryan Fuller[1], Jae N. Lee[1], and Nathaniel Livesey[1]

[1]Jet propulsion Laboratory, California Institute of Technology, Pasadena, California, USA

[2]Goddard Space Flight Center, Global Modeling and Assimilation Office, Greenbelt, Maryland, U.S.A.

Abstract

This paper gives an overview of August 2004 through July 2009 upper tropospheric (UT) water vapor (H_2O) and ice water content (IWC) from the Aura Microwave Limb Sounder (MLS) and comparisons with outputs from the NASA Goddard Earth Observing System Version 5 (GEOS-5) data assimilation system. Both MLS and GEOS-5 show that high values of H_2O and IWC at 215 to 147 hPa are associated with areas of deep convection. They exhibit good (within ~15%) agreement in IWC at these altitudes, but GEOS-5 H_2O is ~50% (215 hPa) to ~30% (147 hPa) larger than MLS, possibility due to its higher temperatures at these altitudes. GOES-5 produces a weaker intertropical convergence zone than MLS, while a seasonally-migrating band of tropical deep convection is clearly evident in both the MLS and GEOS-5 UT H_2O and IWC. MLS and GEOS-5 both show spatial anti-correlation between IWC and H_2O at 100 hPa, where less H_2O is associated with low temperatures in regions of tropical convection. At 100 hPa, GEOS-5 produces 50% less IWC and 15% less H_2O in the tropics, and ~20% more H_2O in the extra-tropics, than does MLS. Behavior of the 100 hPa H_2O, which exhibits a quasi-biennial oscillation, appears consistent with it being controlled by temperature. The seasonal cycle in the vertical transport of tropical mean H_2O from ~147 hPa to ~10 hPa appears much stronger in MLS than in GEOS-5. The UT IWC and H_2O interannual variations, from both MLS and GEOS-5, show clear imprints of the El Niño-Southern Oscillation.

1. Introduction

Upper-tropospheric (UT) water vapor (H_2O) and clouds play important roles in regulating Earth's climate, producing feedbacks to climate forcings by increasing greenhouse gases. H_2O is the primary natural atmospheric greenhouse gas, trapping some of the outgoing longwave radiation (OLR) that would otherwise be emitted to space. The increase of UT H_2O with sea surface temperature (SST) provides a strong positive feedback in response to surface temperature increases that can be caused by increasing anthropogenic greenhouse gases [e.g. *Held and Soden*, 2000; *Su et al.* 2006a]. *Udelhofen and Hartmann* [1995] showed that OLR is mostly sensitive to UT relative humidity changes above 400 hPa. Climate models indicate that UT H_2O could increase ~200% by the end of the 21st century, compared to a ~20% increase in lower tropospheric H_2O [*Soden et al.*, 2005]. This UT amplification underscores the importance of monitoring and quantifying UT H_2O variability.

Clouds in the UT tend to have a net warming effect, as their cold tops result in low OLR [*Stephens*, 1990; *Su et al.*, 2008]. The occurrence of UT clouds is closely related to UT humidity [*Udelhofen and Hartmann*, 1995; *Soden and Fu*, 1995; *Su et al*., 2006a]. The variation of UT cloud amount with SST and the resulting potential climate feedback have been a subject of debate [*Lindzen et al.*, 2001; *Lin et al.*, 2002; *Hartmann and Michelsen*, 2002; *Su et al*., 2008]. The UT cloud radiative heating also influences transport from the troposphere to the stratosphere [e.g. *Corti et al.*, 2006; *Hartmann et al.*, 2001].

The Microwave Limb Sounder (MLS) on board the Aura satellite, launched on July 15, 2004, provides simultaneous global measurements of UT H_2O, cloud ice water content (IWC), temperature (T), and several trace gases [*Waters et al.* 2006]. *Li et al.*

[2005; 2007] compared Aura MLS IWC measurements with European Centre for Medium-range Weather Forecast (ECMWF) analyses and forecasts, and with other state-of-the-art climate model simulations, and found differences as large as factor of 10 between models and observations. These helped promote modifications to the ECMWF model cloud microphysics that resulted in significant improvement [*Waliser, et al.*, 2009]. *Su et al.* [2006] found differences between models and observations of up to a factor of 4 in the relationships among UT H_2O, IWC, and SST. *Read et al.* [2008], using MLS H_2O and CO measurements, estimated the relative influences of convection, "freeze-drying" and extra-tropical mixing on the amount of H_2O entering the stratosphere.

This paper presents an overview of the global distributions and temporal variations for UT IWC and H_2O as seen by MLS from August 2004 through July 2009 (the five-year period for which data are currently available), spatial correlations with deep convection and temperature, and comparisons with output from the Goddard Earth Observing System Version 5 (GEOS-5) data assimilation system. Section 2 describes the datasets, section 3 presents spatial distributions, and section 4 presents temporal variations. Section 5 focuses on the UT response to the El Niño-Southern Oscillation (ENSO). Section 6 gives conclusions and discussion.

2. Data

2.1. Aura MLS UT Water Vapor, Cloud, and Temperature Measurements

We use MLS Version 2.2 (V2.2) Level 2 [*Livesey et al.*, 2007] H_2O, IWC and T datasets, whose validations are described by *Read et al.* [2007], *Wu et al.* [2008], and *Schwartz et al.* [2008], respectively. MLS measures ~3500 vertical profiles per day along a sun-synchronous suborbital track having equatorial crossings at 1:40 PM and 1:40 AM

local solar times. The Level 2 data are produced on pressure surfaces (12 surfaces per decade) from 316 to 0.1 hPa, with IWC having a limited useful range of 215 to 83 hPa. These data have a vertical resolution of ~3-4 km, and horizontal resolutions of ~7 km across-track and ~200-300 km along-track. Estimated measurement accuracies are 20% for H_2O, 2 K for temperature (which, in cloudy regions, has a known low bias of ~2 K at 215 hPa and ~0.5 K at 147 hPa [*Schwartz et al.* 2008]), and a factor of two for IWC.

MLS measurements are generally not degraded by the presence of clouds and aerosols, whose particle sizes are typically much smaller than the measurement wavelengths. Very thick clouds (IWC > ~50 mg/m3) can degrade the temperature and some species measurements [*Wu et al.* 2008], but the retrieval algorithms [*Livesey et al.*, 2006] flag such measurements and they are not used here. See *Wu and Jiang* [2004] for details on the identification and quantification of cloud-affected radiances and the IWC retrieval.

2.2. GEOS-5 Meteorological Products

Meteorological datasets produced by the GEOS Versions 5.1.0 and 5.2.0 data assimilation systems are used in this study. *Rienecker et al.* [2008] describe the meteorological analysis, which uses a three-dimensional variational (3D-Var) approach [*Sasaki*, 1970]. GEOS-5.1.0 ran in near-real time between 17 October 2007 and 14 August 2008; it was also used to retroactively analyze the period from October 2003, before the Aura launch, until October 2007. GEOS-5.1.0 was replaced by GEOS-5.2.0 on 14 August 2008. Both versions, collectively referred to as GEOS-5, produce analyses, forecasts and assimilated fields on a 72-layer grid, extending from the surface to 0.01 hPa, with a $0.5° \times 0.67°$ latitude-longitude resolution. Vertical resolution is ~1.5 km in

the UT. Differences between the two versions of GEOS-5 will be mentioned as necessary in the presentation of results.

The GEOS-5 analyses are "snapshots" of the atmospheric state produced four times daily (at 00Z, 06Z, 12Z, and 18Z) using optimal combinations of model forecasts and many observations [*Rienecker et al.*, 2008] via the Grid-point Statistical Interpolation (GSI) technique of *Wu et al.* [2002]. The assimilated fields are a continuous time series produced using the GEOS-5 atmospheric general circulation model (AGCM), in which an additional forcing term is added to the momentum, thermodynamic, moisture and ozone equations, following *Bloom et al.* [1996]. This "incremental analysis update" (IAU) forcing is computed from the difference between analysis and AGCM forecast at the analysis times, then added as a forcing tendency that remains constant in six-hour segments that straddle the analysis times. The assimilated data are these AGCM fields that are constrained by the analyses and contain all information derived from the model, such as cloud and radiation fields, in addition to the analyzed variables [*Rienecker et al.*, 2008].

The importance of transport to the moisture budget and the fact that all clouds in the GEOS-5 assimilations depend strongly on the AGCM require that some details of the model be mentioned for understanding the products. The GEOS-5 AGCM is coded flexibly, but used in particular configurations (spatial resolution and physical parameter settings) in each version of the assimilation system. Adiabatic transport is computed using the "finite-volume dynamical core" [*Lin*, 2004] with a quasi-Lagrangian vertical coordinate, followed by remapping to the standard 72-layer hybrid grid on which physical tendencies are computed every 30 minutes. The model includes prognostic equations for large-scale gases, liquid (condensate) and ice (anvil-type) water, with

consideration of sub-grid convective contributions to the large-scale liquid and ice phases. Convection is computed using an adaptation of the Relaxed Arakawa-Schubert (RAS) convection code [*Moorthi and Suarez, 1992*], with modifications based on *Sud and Walker* [1999] as described in *Bacmeister et al*. [2006]. RAS considers a sequence of detraining convective plumes extending between cloud base (set as a fixed layer in GEOS-5, but inherently adaptable in RAS) and each layer below the tropopause region (close to 100hPa); each plume produces detraining mass and cloud condensate at each layer and also modifies the environmental meteorological (temperature, moisture, wind) profiles felt by the next plume. The large-scale cloud condensate scheme, based on probability distribution functions (PDFs) of the moisture field assumed inside a grid box, incorporates changes to condensate and anvil clouds obtained from RAS, then computes new sources for the anvil cloud (freezing of existing condensate) and new partitioning of condensate, before computing loss due to evaporation, auto-conversion of liquid or mixed-phase condensate, sedimentation of frozen condensate, and accretion of condensate by falling precipitation. Details of these processes are given in *Rienecker et al*. [2008].

Atmospheric moisture in GEOS-5 is analyzed in the form of relative humidity along with other analysis variables including the stream function, the unbalanced part of velocity potential, temperature, surface pressure, ozone, cloud liquid and ice water, and regression coefficients for radiance bias correction. The optimal analysis is obtained by finding the best fit to the six-hour forecast field and observations while minimizing the cost function. Various observation types such as radiosondes and radiances from the Microwave Humidity Sounder (MHS), the Special Sensor Microwave/Imager (SSM/I) and the Atmospheric Infrared Sounder (AIRS) provide information to constrain the

moisture fields. AIRS, in particular, gives information on vertical structure for atmospheric temperature and moisture due to its sounding capability. A total of 152 spectral channels from AIRS are currently assimilated in GEOS-5; these are selected from the 281-channel "NWP subset" of AIRS radiance measurements. While most of the AIRS channels are subject to water vapor absorption, it is most significant in the infrared portion of the spectrum from 6.20μm to 8.22μm. At present, 49 of the water vapor channels from this band are being assimilated. These water vapor absorption channels peak at different pressure levels in the troposphere, providing information on the vertical distribution of moisture for the analysis. The observation error covariance matrix for radiance data is assumed to be diagonal, i.e., possible inter-channel correlations are neglected. The error values assigned to the water vapor channels are larger than those assigned to temperature channels in order to account for the possibility of inter-channel error correlations, the effects of undetected residual cloud, and the non-linear nature of the moisture channels that is not accounted for in the formulation of Jacobians in the 3D-Var analysis.

For comparison with MLS, the GEOS-5 data are interpolated onto the MLS measurement locations in both space and time. Previous studies [e.g., *Li et al.* 2007; *Su et al.* 2006b] have shown that such interpolation is particularly important because of potential artifacts that arise from incomplete sampling of the diurnal cycle by polar-orbiting satellites. For horizontal sampling, GEOS-5 data are collocated with MLS data by averaging the data in boxes of 3° along the track and 1° across the track centered on the MLS measurement locations (approximately matching the MLS footprints). Vertically, the respective MLS averaging kernels [*Read et al.* 2007, *Schwartz et al.* 2008] are applied to the GEOS-5 H_2O mixing ratio and temperature products. The GEOS-5

IWC data are averaged in vertical boxes of ~3.5 km centered on MLS data points to mimic the MLS IWC vertical resolution [*Wu et al.* 2008].

3. Global distribution of UT H_2O and IWC

3.1. Annual mean maps

Figure 1 shows four-year mean (January 2005 to December 2008) annual IWC, H_2O and T maps at three pressure levels (100, 147, and 215 hPa), from both MLS observations and GEOS-5 analyses. Contours enclosing GEOS-5 OLR of 240 Wm^{-2} or less (indicating regions of deep convection), and potential vorticity contours of 3.5×10^{-6} $Km^2kg^{-1}sec^{-1}$ (PV3.5, indicating the poleward edge of the dynamical tropopause), are superimposed. Both MLS and GEOS-5 data show that at 215 and 147 hPa, large IWC and H_2O and low OLR are collocated in the tropical western Pacific, west central Africa and northern South America. The PV3.5 contour generally encloses the large IWC and H_2O values, supporting the notion [e.g. *Wirth* 1999, *Elbern et al.* 1998] that it generally marks the boundary between tropospheric and stratospheric air. Poleward of the PV3.5 contours, there are relatively few clouds and H_2O concentrations are much smaller. The PV3.5 contours also enclose warm regions at 215 hPa, related to latent heat release from tropical convection, and low T values at 147 and 100 hPa, where adiabatic cooling in upwelling dominates as convective influence extends up to the cold tropopause. Higher stratospheric T values are found poleward of the PV3.5 contour. At 100 hPa, both MLS and GEOS-5 have an H_2O minimum over the Western Pacific, extending somewhat to the east of the lowest OLR and to the north of peak IWC, but coincident with minimum T. The convective regions over equatorial South America and Africa are warmer and moister at 100 hPa than that over the Western Pacific, consistent with the premise that T

controls humidity near the tropical tropopause [*Holton and Gettelman* 2001; *Read et al.* 2004], although convective dehydration may also play a role [*Sherwood and Dessler* 2001].

GEOS-5 IWC and H_2O at 215 hPa are quite similar to MLS fields both in morphology and in magnitude, although GEOS-5 is moister than MLS at this level. GEOS-5 has less 147 hPa IWC and more H_2O than MLS. This might be due to too much sublimation and/or too little condensation in the model's microphysics. GEOS-5 at 100 hPa has smaller values of IWC and is drier in the tropics and wetter in the extra-tropics than MLS. The stronger latitudinal gradient of 100 hPa H_2O in GEOS-5 may indicate some deficiencies in its representation of mass transport from the troposphere to the stratosphere. GEOS-5 is on average warmer than MLS in the tropics by ~3 K at 215 hPa and ~1 K at 147 hPa, which is not unexpected due to the known MLS low biases in cloudy regions (~2 K at 215 hPa and ~0.5 K at 147 hPa, *Schwartz et al.* [2008]). MLS and GEOS-5 tropical 100 hPa temperatures agree to within ~0.5 K.

Figure 2 shows the 4-year (January 2005 to December 2008) tropical (15°S-15°N) mean profiles of IWC, H_2O and T from both MLS and GEOS-5, along with their daily standard deviations from the 5-year mean. The GEOS-5 IWC profile agrees within 12% with MLS at 215 hPa to 147 hPa but becomes 30%, 50% and 70% smaller than the MLS IWC at 121 hPa, 100 hPa and 83 hPa, respectively. Although these are all within the estimated (factor of 2) uncertainty of MLS measurements, the smaller GEOS-5 IWC amounts above 147 hPa suggest that convection in the model does not extend to sufficiently high altitudes.

The GEOS-5 and MLS differences in tropical H_2O and T appear to have a source other than that for the IWC differences. GEOS-5 H_2O is limited to values corresponding

to 100% or less relative humidity, and an overestimate of T could possibly lead to an overestimate of H_2O. Figure 2 shows that, after accounting for the known MLS ~2 K cold bias, GEOS-5 215 and 178 hPa tropical T is still larger than that of MLS by ~1 K, which may contribute to the large H_2O in GEOS-5 at the two levels. However, the saturation H_2O mixing ratio profile computed using GEOS-5 T suggests that this can not explain the H_2O discrepancy between MLS and GEOS-5 at 147 hPa altitude and above. In summary, GEOS-5 215 hPa tropical H_2O is larger than that of MLS by ~50% and 215 hPa T is larger by ~3.5 K, both of which are significant compared to estimated MLS measurement uncertainties. GEOS-5 and MLS tropical 147 hPa H_2O agree within ~30% (only slightly larger than the estimated 20% MLS measurement uncertainty) and 147 hPa T agree to ~0.2 K (within the MLS measurement uncertainty). GEOS-5 and MLS tropical 100 hPa H_2O agree to ~15% and T to 0.2 K (both within the MLS measurement uncertainty).

3.2. Seasonal maps

Figure 3 shows seasonal MLS IWC and H_2O maps at 100, 147 and 215 hPa. The overlaid 240-Wm^{-2} contour generally encloses the highest values of both IWC at all three pressure levels and H_2O at 147 and 215 hPa. High IWC in December to February (DJF) is concentrated south of the Equator in central-south Africa, the Western Pacific and South America. In June-August (JJA), the maximum IWC is distributed over the South Asian monsoon region, while South American convection has shifted northward to cover Central America. Seasonal variations over the Western Pacific are relatively small. The seasonal variation of the ITCZ (Inter-Tropical Convection Zone) and IPCZ (Inter-Pacific Convection Zone) is also apparent in MLS IWC.

At 215 hPa, maxima in both IWC (Figure 3a) and H_2O (Figure 3b) are collocated with low OLR, indicating convective moistening of the UT in all seasons. At 147 hPa, the

H_2O maxima are over the western Pacific in DJF, and over southern Asia in JJA, in both cases slightly north of the strongest convection. Studies using MLS data [e.g. *Fu et al.* 2006; *Park et al*. 2007] have shown convectively-lofted H_2O is trapped in the strong anti-cyclone over the Tibetan Plateau during the Asian summer monsoon, where IWC and H_2O are seen distributed across the tropopause (PV3.5 contour) into the lower stratosphere. At 100 hPa, the minimum H_2O values are found in the cold region over the tropical western Pacific in all four seasons.

Comparing MLS and GEOS-5 maps (shown in Supplemental Figure 1), there is overall similarity in both IWC and H_2O in terms of seasonal variations, with the differences shown in Figures 1 and 2 also evident in the seasonal maps. However, GEOS-5 shows a much less evident IWC ITCZ feature than MLS, especially in DJF and JJA. This is thought to be due to GEOS-5 underestimating the height of convective penetration, as has been mentioned earlier. We note, however, that GEOS-5 has less discrepancy with MLS than GEOS-4.

4. Time evolution of UT H_2O and IWC

4.1. Latitude-time evolution

Latitude-time sections of zonal-mean IWC and H_2O from MLS (Figure 4a) and GEOS-5 (Figure 4b) further illustrate the seasonal evolution from August 2004 to July 2009. The patterns of evolution of 215 and 147 hPa H_2O and IWC, as well as 100 hPa IWC are qualitatively similar, while the 100 hPa H_2O pattern is noticeably different in both MLS and GEOS-5. At 215 and 147 hPa in MLS and GEOS-5, the meridional movements of high IWC and H_2O are in phase and follow the Sun, with highest IWC and H_2O in the northern summer. While the GEOS-5 147 and 215 hPa IWC are in acceptable agreement (within ~15%) with MLS, the GEOS-5 147 and 215 hPa H_2O maxima are

larger than MLS by ~30% to 50% throughout the year, as is also evident in Figure 1. MLS 100 hPa IWC is confined to a narrow latitudinal band, which shifts seasonally in a similar way to 215 and 147 hPa IWC. The underestimate of 100 hPa IWC in GEOS-5 compared to MLS is clearly a year-round feature. The seasonal cycle in 100 hPa H_2O is dramatically different from that at 147 and 215 hPa. The 100 hPa H_2O is correlated with the annual cycle of temperature, with minima occurring over the Equator in boreal winter and spring. Annual maxima occur more or less simultaneously in both hemispheres (around August), with larger values of 100 hPa H_2O in the northern hemisphere (NH) than in the southern hemisphere (SH). GEOS-5 NH (0°-60°N mean) 100 hPa H_2O values are lower than MLS by ~20%. In the SH (0°-60°S), GEOS-5 shows larger H_2O (~20% larger than MLS) which also persists longer throughout the year than in the NH. This is most likely due to problems in the model related to relaxation to a constant moisture mixing ratio in the stratosphere, which may not be related to the moist physical processes in the troposphere.

There may be evidence for a two-year cycle in the magnitude of the H_2O minimum at 100 hPa in both MLS and GEOS-5, which could be a manifestation of the tropical biennial oscillation (TBO) [e.g. *Li et al.* 2001]. Longer-term data are needed to determine if this is really the case.

4.2. Height-time evolution

Figure 5a shows the height-time section of tropical (15°S-15°N) daily mean MLS H_2O anomalies from the 5-year (August 2004 to July 2009) mean, illustrating the so-called "tape-recorder" signal [*Mote et al.* 1996]. There is a clear vertical transport of H_2O from 121 hPa through the stratosphere. An apparent two-year cycle in the magnitude of the tape-recorder signal, particularly evident in the magnitude of the boreal-winter minimum

around 100 hPa, may be related to the quasi biennial oscillation (QBO) [e.g. *Baldwin et al.*, 2001] or TBO [e.g. *Li et al.* 2001]. H_2O signals imprinted at the bottom of the stratosphere are maintained through the stratosphere for 12 to 18 months as the air rises. The tape recorder is less clear in the upper stratosphere, although the two intense dry phases are especially evident up to ~1 hPa. The seasonal cycle of tropical GEOS-5 H_2O (Figure 5b) near 100 hPa has a similar magnitude to that of MLS. The amplitude of the GEOS-5 annual cycle at pressures below 68 hPa drops more rapidly than that of MLS, although the ascent rates are quite similar. This attenuation of the signal in GEOS-5 arises because of its relaxation of stratospheric moisture to a constant value close to 6 ppmv. Such a tape recorder signal does not appear in the IWC field, since the warmer stratosphere quickly sublimates ice particles, and ice is subject to sedimentation.

4.3. Longitude-time evolution

Figure 6 shows the longitude-time section of tropical (15°S-15°N) mean MLS IWC and H_2O anomalies, relative to monthly mean data. On inter-annual time scales, El Niño-Southern Oscillation (ENSO) related signals dominate the variability. The El Niño (warm phase) patterns at 215 hPa (Figure 6b) are characterized by an enhancement of IWC and H_2O in the eastern Pacific accompanied by a reduction of IWC and H_2O in the western Pacific from late 2004 to early 2005 and late 2006 to early 2007. The opposite patterns are seen during the cold La Niña phase from late 2007 to early 2008 and late 2008 to early 2009. IWC anomalies at 100 hPa (Figure 6a) appear in phase with those at 215 hPa, but the H_2O anomalies at 100 hPa are out of phase with the 215 hPa IWC and H_2O. The H_2O anomalies at 100 hPa are less localized in longitude than the IWC anomalies, and are strongest over the Indian Ocean (also see Figure 8 later in section 5). GEOS-5 IWC and H_2O data (see Supplemental Figure 2) show a similar pattern.

5. The UT response to ENSO

The MLS simultaneous and collocated measurements of H_2O, IWC and T provide an unprecedented characterization of the UT response to ENSO variations. Figure 7 shows time series of monthly mean Niño 3.4 SST (defined by *Trenberth* [1997] as the SST averaged for longitudes 170°-240° and latitudes 5°S-5°N), and the tropical (15°S to 15°N) mean MLS IWC and H_2O at 100, 147, and 215 hPa. The time series of tropical mean IWC and H_2O anomalies have similar time evolution to that of the Niño 3.4 SST. We choose DJF 2005 and 2008 to represent, respectively, the warm and cold phases of ENSO. Figures 8a and b show the corresponding IWC, H_2O and T anomalies for the two phases. A typical dipole pattern [*Semazzi and Indeje*, 1999] is seen in IWC and H_2O at 215 and 147 hPa, with positive anomaly in the central-eastern Pacific and negative anomaly in the western Pacific during El Niño and the opposite pattern during La Niña. At 100 hPa in DJF 2005, a positive IWC anomaly and a negative H_2O anomaly in the central eastern Pacific are accompanied by anomalies of opposite sign in the western Pacific. The opposite signatures are evident in DJF 2008. The negative IWC anomaly over the western Pacific during El Niño is an indication of reduced convection in response to warmer SST in the central-eastern Pacific [*Su et al.*, 2002]. This is possibly associated with anticyclones west of the localized SST heating, as suggested by *Highwood and Hoskins* [1998]. The 100 hPa H_2O anomalies are particularly strong in the Indian Ocean. Whether these particularly strong anomalies represent a teleconnection through "atmospheric bridge" [*Alexander et al.*, 2002; *Klein et al.*, 1999] or a response to local SST anomaly is not clear. The ENSO response in GEOS-5 (see Supplemental Figure 3 and Figure 4) is similar to that of MLS.

6. Summary and Conclusions

We have presented Aura MLS UT H_2O and IWC measurements made from August 2004 through July 2009, with comparisons to GEOS-5 analyses of these quantities for the same period. The global distributions of four-year-mean annual and seasonal averages, and tropical temporal evolution and response to ENSO, are given. Some comparisons with MLS and GEOS-5 UT temperatures are also discussed.

Agreement between MLS and GEOS-5 H_2O at 100 and 147 hPa is generally within the estimated MLS measurement accuracy of ~20% (albeit slightly, but probably not significantly, worse, ~30%, at 147 hPa). GEOS-5 has (during all seasons) smaller minimum tropical 100 hPa H_2O values, and moister extratropics, than MLS, thought to be caused by the model's relaxation to fixed stratospheric H_2O concentrations. GEOS-5 215 hPa H_2O is larger than MLS by ~50%, probably because the GEOS-5 deep convection does not extend sufficiently high. IWC agreement is within the factor of 2 estimated accuracy of MLS, but comparisons of IWC vertical distributions also suggest that GEOS-5 deep convection does not extend sufficiently high. There appears to be a significant difference in 215 hPa temperature, with GEOS-5 being ~1 K warmer after accounting for the known ~2 K cold bias in MLS. MLS and GEOS-5 147 and 100 hPa temperatures agree on average to within ~0.2 K, well within the MLS uncertainty.

The tropical distributions of 215 hPa H_2O and IWC are positively correlated; large values of both are associated with regions of deep convection, as previously found [e.g. *Su et al.* 2006a]. The distributions of 100 hPa H_2O and IWC are negatively correlated, with less H_2O and more IWC in regions of deep convection, as expected from "freeze-drying" of uplifted air. The transition from positive to negative correlation occurs

between 147 and 100 hPa. The tropical 215 hPa H_2O and IWC seasonal variations track regions of deep convection, while the 100 hPa H_2O seasonal variations track 100 hPa cold regions. The largest values of tropical H_2O occur in the northern summer over the South Asia monsoon region; the smallest values of H_2O occur in the northern winter over the western Pacific.

Tropical zonal mean H_2O and IWC exhibit strong seasonal and interannual variations. There is an indication of a two-year cycle in the tropical UT boreal winter H_2O minimum, possibly related to the roughly two-year oscillation (TBO) in tropical SST [*Li et al.* 2001]. The stratospheric H_2O tape-recorder signal displays a two-year cycle, which may be related to the QBO [*Baldwin et al.*, 2001]. GEOS-5 H_2O appears to ascend faster through the upper tropical tropopause (121 hPa – 83 hPa,) than does MLS H_2O, and has a smaller amplitude seasonal cycle in the stratosphere (where moisture is relaxed to a constant value). A future GEOS objective is to implement a more realistic stratospheric moisture module having methane oxidation chemistry.

Fluctuations in tropical UT H_2O and IWC are associated with moderate El Niño and La Niña events that occurred during the 5-year period analyzed here. H_2O and IWC zonal mean fractional anomalies were ~10%. The IWC and H_2O deseasonalized 215 hPa anomalies exhibit a dipole pattern during El Niño (La Niña), with positive (negative) anomalies in the eastern Pacific and negative (positive) anomalies in the western Pacific. A strong positive (negative) 100 hPa H_2O anomaly occurs over the Indian Ocean during El Niño (La Niña).

Acknowledgements

The authors acknowledge the support from the Aura MLS project, Jet Propulsion Laboratory (JPL), California Institute of Technology, conducted under contract with NASA. We also acknowledge the support by NASA's Modeling and Analysis Program (MAP) for the Global Modeling and Assimilation Office at NASA Goddard Space Flight Center. The GEOS-5 data assimilation system is run on NASA's High-Performance Computing (HEC) resources at NASA's Goddard and Ames Research Centers.

Figure Caption

Figure 1: Annual mean IWC, H_2O and temperature maps at 100, 147 and 215 hPa pressure levels from MLS observations (upper panels) and GEOS-5 analyses (lower panels). The black contour is the GEOS-5 OLR at 240 Wm^{-2}. The grey contour is the GEOS-5 PV3.5. The GEOS-5 data are averaged onto 3°×1° boxes centered on MLS measurement locations. MLS averaging kernels are applied to GEOS-5 H_2O and temperature data, and GEOS-5 IWC data are also vertically averaged in 3.5 km boxes centered on MLS data points. Four years of data from January 2005 to December 2008 are used to compute the averages shown in this Figure. Thus this is a four-year average of "annual mean".

Figure 2: Tropical (15°S-15°N) mean IWC, H_2O and T profiles from both MLS (black) and GEOS-5 (blue). The profiles are averages of daily mean tropical profiles from January 2005 to December 2008. The standard deviations of daily profiles for MLS (gray-shade) and GEOS-5 (blue-dashed) are also shown, as well as the saturation specific humidity profile (red) computed using the GEOS-5 Temperature.

Figure 3: Seasonal mean MLS IWC (a) and H_2O (b) maps at 100, 147 and 215 hPa pressure levels. The black contour is the GEOS-5 OLR at 240 Wm^{-2}. The grey contour is the GEOS-5 PV3.5. Data from December 2004 to October 2008 are used to compute the seasonal averages shown here. Each season includes 3-month from four different years. For example, JJA seasonal map is the average of June-August 2005, June-August 2006, June-August 2007, and June-August 2008; DJF seasonal map is the average of December 2004-February 2005, December 2005-February 2006, December 2006-February 2007, and December 2007-February 2008.

Figure 4: Latitude-time sections of zonal-mean IWC and H_2O at 100, 147 and 215 hPa from (a) MLS observations and (b) GEOS-5 analyses, computed from daily zonal mean data.

Figure 5: Height-time section of tropical (15°S-15°N) mean H_2O anomalies from MLS (a) and GEOS-5 (b), computed from daily tropical mean data. MLS H_2O vertical averaging kernels are not applied to GEOS-5 H_2O in this plot.

Figure 6: Longitude-time section of tropical (15°S-15°N) mean MLS IWC and H_2O anomalies at 100 hPa (a) and 215 hPa (b), computed from monthly mean data.

Figure 7: Time series of monthly mean SST (top panels) in the Niño 3.4 region (longitude 170°-240° and latitude 5°S-5°N), and (lower panels) monthly tropical (15°S-15°N) mean MLS IWC and H_2O.

Figure 8: Maps of 2005 DJF and 2008 DJF anomalies of IWC, H_2O and T from MLS measurements. The anomalies are computed as the difference between 2005 or 2008 DJF averages and the four-year (2005-2008) average. Note that the 2005 DJF covers three months from December 2004 to February 2005, while the 2008 DJF refers to December 2007 to February 2008 period.

References:

Alexander, M.A., I. Blade, M. Newman, J.R. Lanzante, N.C. Lau, and J.D. Scott (2002), The atmospheric bridge: The influence of ENSO teleconnections on air–sea interaction over the global oceans. *J. Climate*, 15, 2205-2231.

Bacmeister, J. T, M. J., Suarez, F. R. Robertson (2006), Rain re-evaporation, Boundary Layer–Convection interactions, and Pacific rainfall patterns in an AGCM. *J. Atmos. Sci.*, 62, 3383–3403.

Baldwin, M.P. et al. (2001), The Quasi-Biennial Oscillation. *Rev. Geophys.,* 39, 179–229.

Bloom, S., L. Takacs, A. DaSilva, and D. Ledvina (1996), Data assimilation using incremental analysis updates. *Mon. Wea. Rev.*, **124**, 1256-1271.

Corti, T., B.P. Luo, Q. Fu, H. Vömel, and T. Peter (2006), The impact of cirrus clouds on tropical troposphere-to-stratosphere transport, *Atmos. Chem. Phys.*, 6, 2539–2547.

Elbern, H., J. Hendricks and A. Ebel (1998), A Climatology of Tropopause Folds by Global Analyses, *Theoretical and Applied Climatology*, Publisher: Springer Wien, Volume 59, Numbers 3-4 / May, 1998, DOI 10.1007/s007040050023, pp 181-200.

Fu, R., Y. Hu, J.S. Wright, J.H. Jiang, R.E. Dickinson, M. Chen, M. Filipiak, W.G. Read, J.W. Waters, and D.L. Wu (2006), Short circuit of water vapor and polluted air to the global stratosphere by convective transport over the Tibetan Plateau, *Proc. Nat. Acad. Sci.* 103, 5664-5669.

Fueglistaler, S., A. E. Dessler, T. J. Dunkerton, I. Folkins, Q. Fu, P. W. Mote (2009), Tropical tropopause layer, *Rev. Geophys.*, 47, RG1004, doi:10.1029/2008RG000267.

Hartmann, D. L. and M. L. Michelsen (2002), No Evidence for Iris. *Bull. Amer. Meteor. Soc.*, 83, 249-254.

Hartmann, D. L., J. R. Holton, and Q. Fu (2001), The heat balance of the tropical tropopause, cirrus, and stratospheric dehydration. *Geophys. Res. Lett.*, 28, 1969–1972.

Held, I. H., and B. J. Soden (2000): Water vapor feedback and global warming. *Annu. Rev. Energy Environ.* 25, 441-475.

Highwood, E.J., B. J. Hoskins (1998), The tropical tropopause, *Quarterly Journal of the Royal Meteorological Society,* 124(549): 1579.

Holton, J. R. and A. Gettelman (2001), Horizontal transport and the dehydration of the stratosphere, *Geophys. Res. Lett.*, 28, 2799–2802.

Klein, S. A., B. J. Soden, and N.-C. Lau (1999), Remote sea surface variations during ENSO: evidence for a tropical atmospheric bridge. *J. Climate*, 12, 917-932.

Koster, R. D., M. J. Suárez, A. Ducharne, M. Stieglitz, and P. Kumar (2000), A catchment-based approach to modeling land surface processes in a GCM, Part 1, Model Structure. *J. Geophys. Res.*,105, 24809-24822.

Li, T., C.-W. Tham, and C.-P. Chang (2001), A coupled air-sea-monsoon oscillator for the tropospheric biennial oscillation. *J. Climate*, 14, 752-764.

Li, J-L., J.H. Jiang, D.E. Waliser, and A.M. Tompkins (2007), Assessing Consistency between EOS MLS and ECMWF Analyzed and Forecast Estimates of Cloud Ice, *Geophys. Res. Lett.* 34, L08701, doi:10.1029/2006GL029022.

Li, J-L., D.E. Waliser, J.H. Jiang, D.L. Wu, W.G. Read, J.W. Waters, A.M. Tompkins, L.J. Donner, J-D. Chern, W-K. Tao, R. Atlas, Y. Gu, K.N. Liou, A. Del Genio, M. Khairoutdinov, and A. Gettleman (2005), Comparisons of EOS MLS Cloud Ice Measurements with ECMWF analyses and GCM Simulations: Initial Results," *Geophys. Res. Lett.* 32, L18710, doi:10.1029/2005GL023788.

Lin, S.-J. (2004), A vertically Lagrangian Finite-Volume Dynamical Core for Global Models. *Mon. Wea. Rev.*, 132, 2293-2307.

Livesey, N. J., et al. (2007), EOS MLS version 2.2 Level 2 data quality and description document, *Tech. Rep. JPL D-33509*, Jet Propul. Lab., Pasadena, Calif.

Livesey, N.J., W.V. Snyder, W.G. Read, and P.A. Wagner, Retrieval algorithms for the EOS Microwave Limb Sounder (MLS) instrument (2006), *IEEE Trans. Geosci. Remote Sensing* 44, no. 5, 1144-1155.

Lin B., B. Wielicki, L. Chambers, Y. Hu, and K.-M. Xu (2002), The iris hypothesis: A negative or positive cloud feedback? *J. Climate*, 15, 3–7.

Lindzen, R.S., M-D Chou, and A. Y. Hou (2001), Does the Earth have an adaptive infrared iris? *Bull. Amer. Meteor. Soc.*, 82, 417-432.

Moorthi, S., and M.J. Suarez (1992), Relaxed Arakawa-Schubert, A Parameterization of Moist Convection for General-Circulation Models. *Mon. Wea. Rev.* **120**, 978-1002.

Mote, P.W., K.H. Rosenlof, M.E. McIntyre, E.S. Carr, J.R. Holton, J.S. Kinnersley, H.C. Pumphrey, J.M. Russell III, J.W. Waters, and J.C. Gille (1994), An atmospheric tape recorder: the imprint of tropical tropopause temperatures on stratospheric water vapor, *J. Geophys. Res.* 101, D2, 3989-4006.

Park, M., W.J. Randel, A. Gettleman, S.T. Massie, and J.H. Jiang (2007), Transport above the Asian summer monsoon anticyclone inferred from Aura MLS tracers, *J. Geophys. Res*. 112, D16309, doi:10.1029/2006JD008294.

Read, W.G., M.J. Schwartz, A. Lambert, H. Su, N.J. Livesey, W.H. Daffer, and C.D. Boone (2008), The roles of convection, extratropical mixing, and in situ freeze-drying in the tropical tropopause layer, *Atmos. Chem. Phys.* 8, 6051-6067.

Read, W.G. et al. (2007), Aura Microwave Limb Sounder upper tropospheric and lower stratospheric H_2O and relative humidity with respect to ice validation, *J. Geophys. Res.* 112, D24S35, doi:10.1029/2007JD008752.

Read, W. G., D. L. Wu, J. W. Waters, and H. C. Pumphrey, (2004), Dehydration in the tropical tropopause layer: Implications from the UARS Microwave Limb Sounder, *J. Geophys. Res.*, 25 109, D06110, doi:10.1029/2003JD004056, 2004.

Rienecker, M.M., M.J. Suarez, R. Todling, J. Bacmeister, L. Takacs, H.-C. Liu, W. Gu, M. Sienkiewicz, R.D. Koster, R. Gelaro, I. Stajner, and J.E. Nielsen (2008), "The GEOS-5 Data Assimilation System - Documentation of Versions 5.0.1, 5.1.0, and 5.2.0 " Technical Report Series on Global Modeling and Data Assimilation, Volume 27, *Max J. Suarez (Ed.),* NASA/TM–2008–104606, Vol. 27.

Sasaki, Y. (1970), Some basic formalisms in numerical variational analysis. *Mon. Wea. Rev.*, 98, 875-883.

Schwartz, M.J. et al. (2008), Validation of the Aura Microwave Limb Sounder Temperature and Geopotential Height Measurements, *J. Geophys. Res.* 113, D15S11, doi:10.1029/2007JD008783.

Semazzi F. H. M., and Indeje, M. (1999), Inter-seasonal variability of ENSO rainfall signal over Africa. *J. Afri. Meteorol. Soc*. 4, 81-94.

Sherwood, S. C. and A. E. Dessler (2001), A model for transport across the tropical tropopause, *J. Atmos. Sci*., 58, 765–779.

Soden, B. J., D. L. Jackson, V. Ramaswamy, M. D. Schwarzkopf, and X. Huang (2005), The radiative signature of upper tropospheric moistening. *Science*, 310(5749), 841-844.

Soden, B. J., and R. Fu (1995), A satellite analysis of deep convection, upper-tropospheric humidity, and the greenhouse effect. *J. Climate*, 8(10), 2333-2351.

Su, H., and J. D. Neelin, (2002), Teleconnection mechanisms for tropical Pacific descent anomalies during El Nino, *J. Atmos. Sci.,* 59, 2682-2700.

Su, H., W.G. Read, J.H. Jiang, J.W. Waters, D.L. Wu, and E.J. Fetzer (2006a), Enhanced positive water vapor feedback associated with tropical deep convection: New evidence from Aura MLS, *Geophys. Res. Lett.* 33, L05709, doi:10.1029/2005 GL025505.

Su, H., D.E. Waliser, J.H. Jiang, J-L. Li, W.G. Read, J.W. Waters, and A.M. Tompkins (2006), Relationships of upper tropospheric water vapor, clouds and SST: MLS observations, ECMWF analyses and GCM simulations, *Geophys. Res. Lett.* 33, L22802, doi:10.1029/2006GL027582.

Su, H., J.H. Jiang, G.L. Stephens, D.G. Vane, and N.J. Livesey (2009), Radiative effects of upper tropospheric clouds observed by Aura MLS and CloudSat, G*eophys. Res. Lett.* 36, L09815, doi:10.1029/2009GL037173.

Sud, Y., and G.K. Walker, 1999: Microphysics of Clouds with the Relaxed Arakawa Schubert Scheme (McRAS). Part I: Design and Evaluation with GATE Phase III Data. *J. Atmos. Sci.,* **56**, 3196-3220.

Trenberth, K. E. (1997), The Definition of El Niño. *Bull. Amer. Meteor. Soc*., 78, 2771-2777.

Udelhofen, P. M., and D. L. Hartmann (1995), Influence of tropical cloud systems on the relative humidity in the upper troposphere. *J. Geophys. Res.*, 100, 7423–7440.

Waliser, D.E., J.F. Li, C.P. Woods, R.T. Austin, J. Bacmeister, J. Chern, A. Del Genio, J.H. Jiang, Z. Kuang, H. Meng, P. Minnis, S. Platnick, W. B Rossow, G. L Stephens, S. Sun-Mack, W-K. Tao, A.M. Tompkins, D.G. Vane, C. Walker, and D. Wu (2009), Cloud ice: A climate model challenge with signs and expectations of progress, *J. Geophys. Res.* 114, D00A21, doi:10.1029/2008JD010015 , 2009.

Waters, J.W. et al. (2006), The Earth Observing System Microwave Limb Sounder (EOS MLS) on the Aura satellite, *IEEE Trans. Geosci. Remote Sensing,* 44, 1075– 1092.

Wirth, V. (1999), Thermal versus dynamical tropopause in upper-tropospheric balanced flow anomalies, *The Quarterly Journal of the Royal Meteorological Society*, Volume 126 Issue 562, pp 299 – 317.

Wu, D. L., and J.H. Jiang, EOS MLS Algorithm Theoretical Basis for Cloud Measurements (2004), *Tech. Rep. JPL D-19299,* Jet Propul. Lab., Pasadena, Calif.

Wu, D.L., J.H. Jiang, and C.P. Davis (2006), EOS MLS cloud ice measurements and cloudy-sky radiative transfer model, *IEEE Trans. Geosci. Remote Sensing* 44, no. 5, 1156-1165.

Wu, D.L., J.H. Jiang, W.G. Read, R.T. Austin, C.P. Davis, A. Lambert, G.L. Stephens, D.G. Vane, and J.W. Waters (2008), Validation of the Aura MLS Cloud Ice Water Content (IWC) Measurements, *J. Geophys. Res.* 113, doi:10.1029/2007JD008931.

Wu, W.-S., R.J. Purser and D.F. Parrish (2002), Three-dimensional variational analysis with spatially inhomogeneous covariances. *Mon. Wea. Rev.*, 130, 2905-2916.

Supplementary Figure 1: Similar to Figure 3 but with GEOS-5 data.

Supplementary Figure 2: Similar to Figure 6 but with GEOS-5 data.

Supplementary Figure 3: Similar to Figure 7 but with GEOS-5 data.

Supplementary Figure 4: Similar to Figure 8 but with GEOS-5 data.

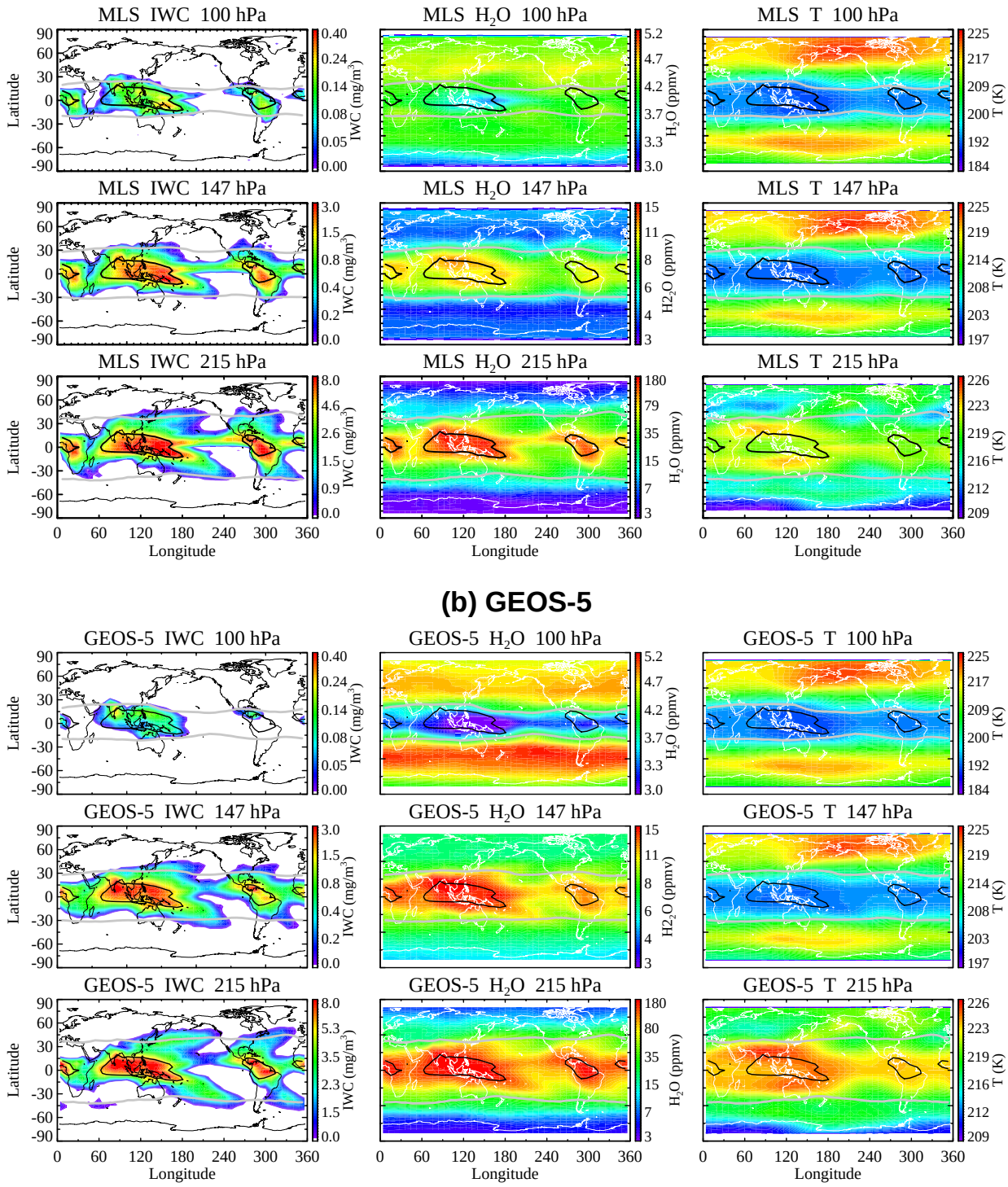
(a) MLS
MLS IWC 100 hPa
MLS H2O 100 hPa
MLS T 100 hPa
MLS IWC 147 hPa
MLS H2O 147 hPa
MLS T 147 hPa
MLS IWC 215 hPa
MLS H2O 215 hPa
MLS T 215 hPa
(b) GEOS-5
GEOS-5 IWC 100 hPa
GEOS-5 H2O 100 hPa
GEOS-5 T 100 hPa
GEOS-5 IWC 147 hPa
GEOS-5 H2O 147 hPa
GEOS-5 T 147 hPa
GEOS-5 IWC 215 hPa
GEOS-5 H2O 215 hPa
GEOS-5 T 215 hPa
Latitude
Longitude
IWC (mg/m3)
H2O (ppmv)
T (K)

Figure 1

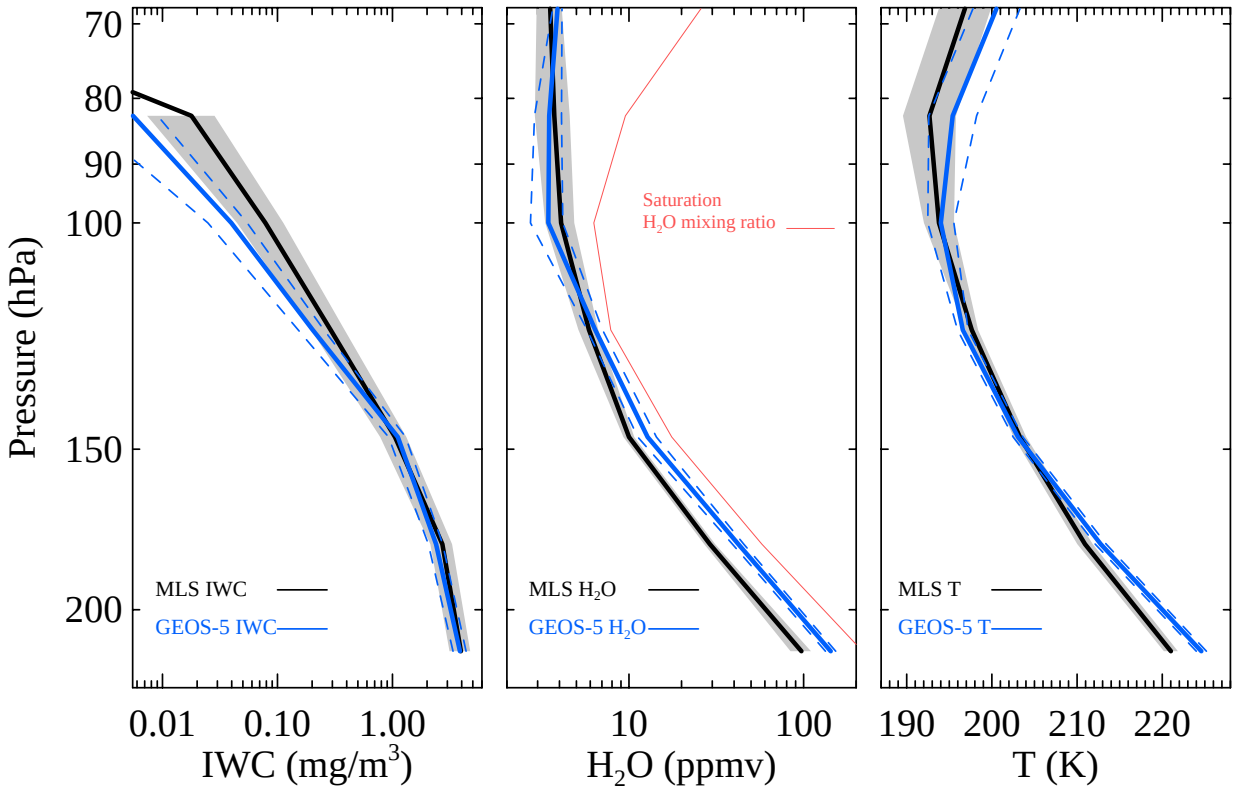
Pressure (hPa)
70
80
90
100
150
200
MLS IWC
GEOS-5 IWC
0.01
0.10
1.00
IWC (mg/m3)
Saturation
H2O mixing ratio
MLS H2O
GEOS-5 H2O
10
100
H2O (ppmv)
MLS T
GEOS-5 T
190
200
210
220
T (K)

Figure 2

(a) MLS IWC

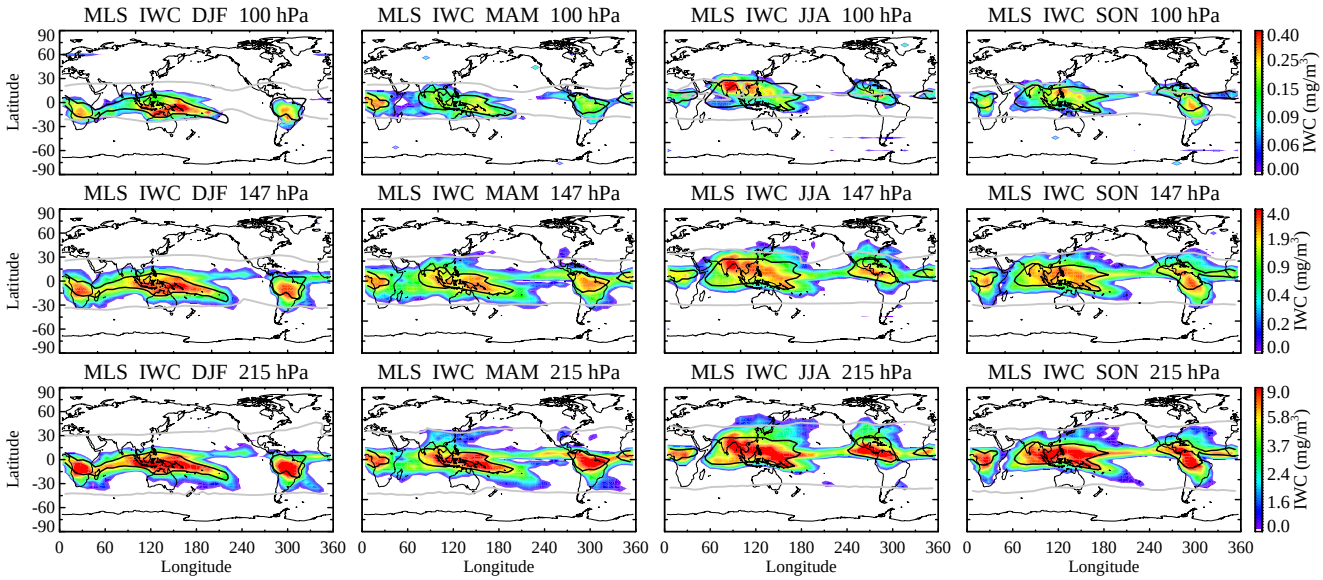

(b) MLS H_2O

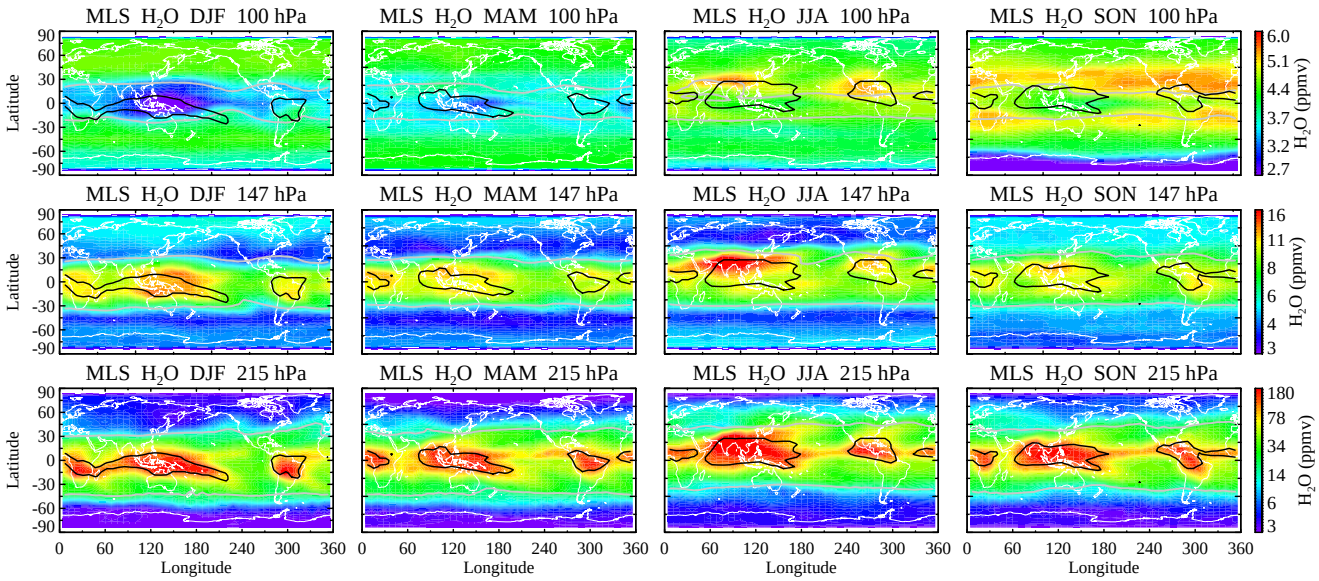

Figure 3

(a) MLS

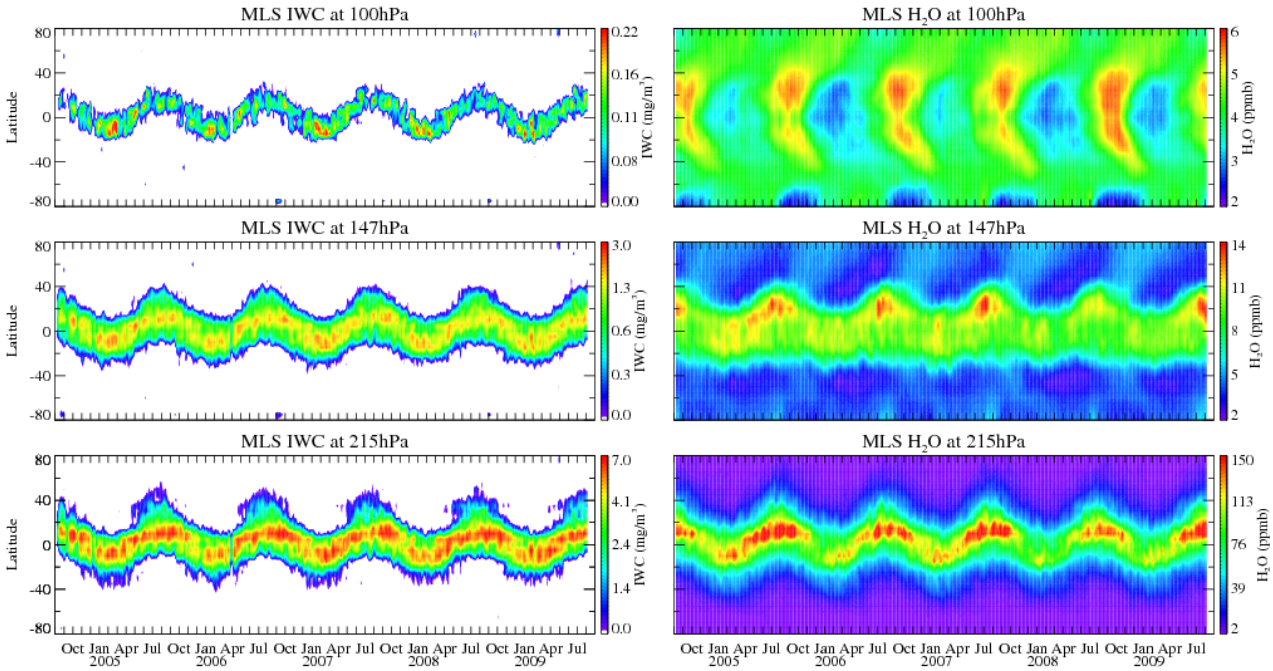

(b) GEOS-5

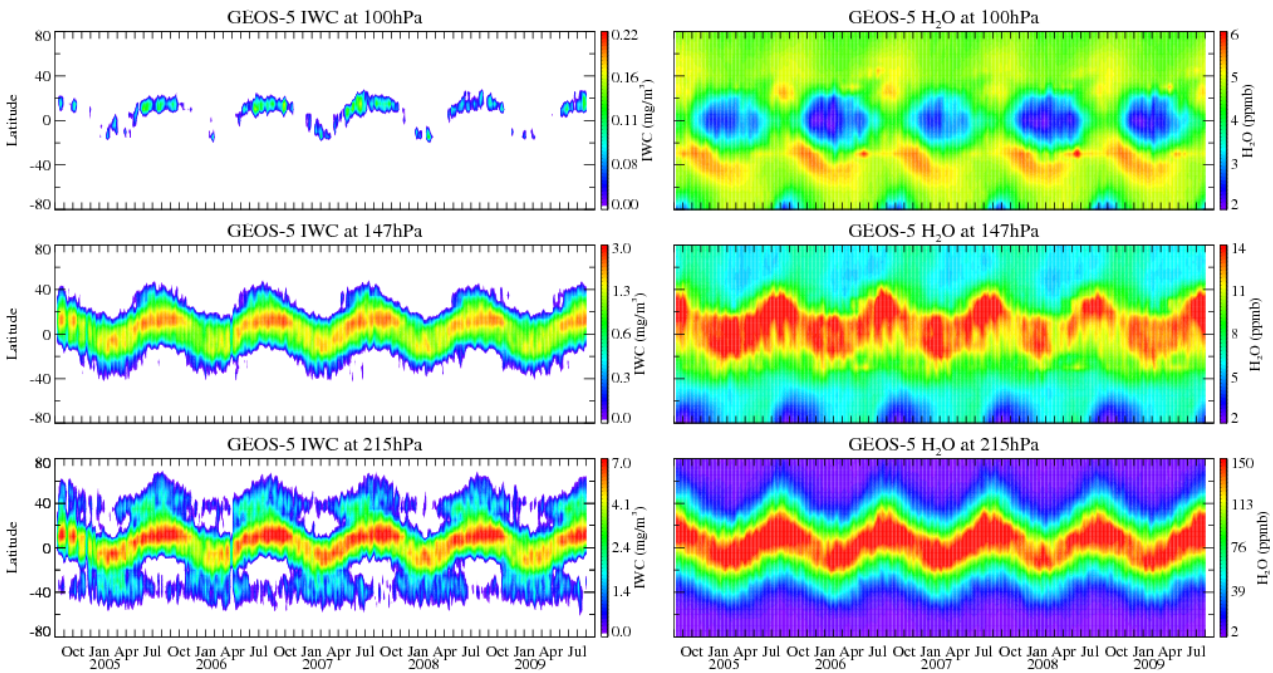

Figure 4

(a)

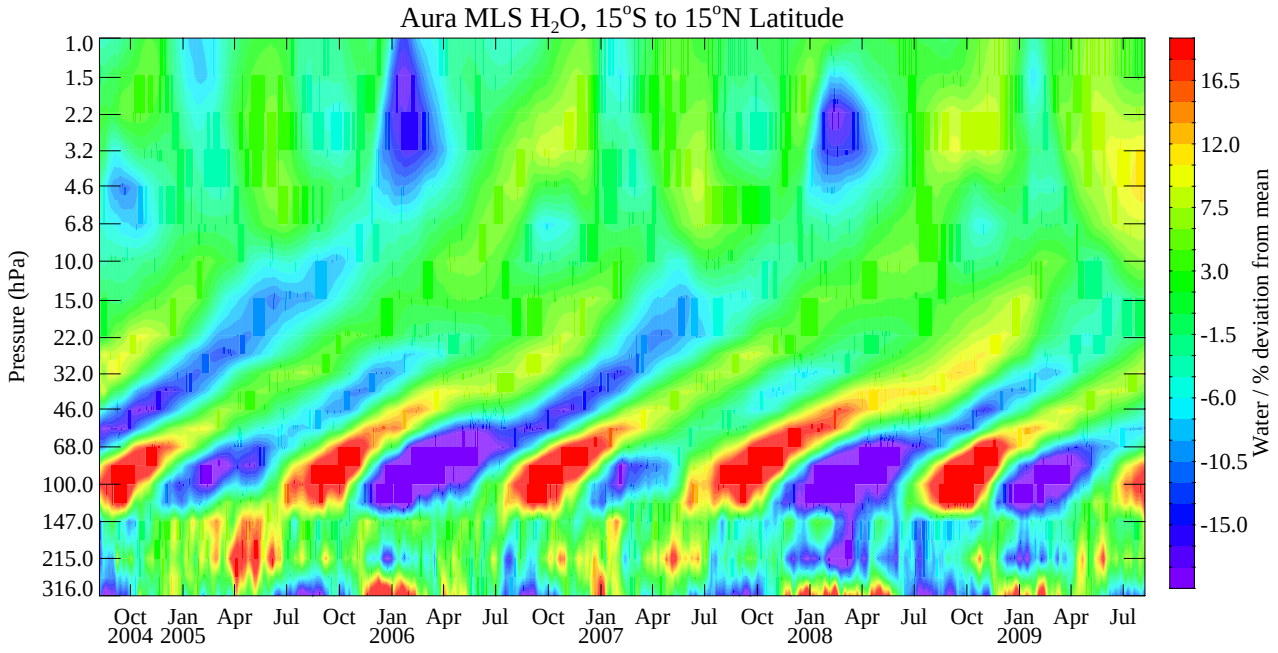
Aura MLS H2O, 15°S to 15°N Latitude
Pressure (hPa)
1.0
1.5
2.2
3.2
4.6
6.8
10.0
15.0
22.0
32.0
46.0
68.0
100.0
147.0
215.0
316.0
Oct 2004
Jan 2005
Apr
Jul
Oct
Jan 2006
Apr
Jul
Oct
Jan 2007
Apr
Jul
Oct
Jan 2008
Apr
Jul
Oct
Jan 2009
Apr
Jul
16.5
12.0
7.5
3.0
-1.5
-6.0
-10.5
-15.0
Water / % deviation from mean

(b)

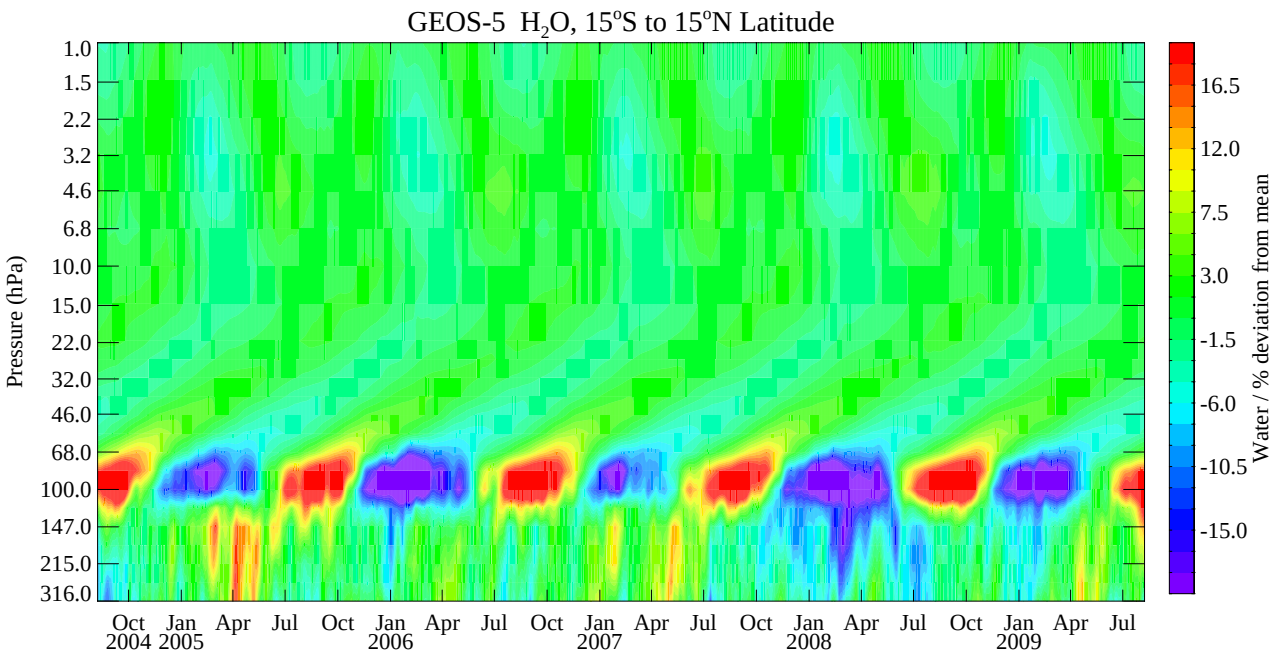
GEOS-5 H2O, 15°S to 15°N Latitude
Pressure (hPa)
1.0
1.5
2.2
3.2
4.6
6.8
10.0
15.0
22.0
32.0
46.0
68.0
100.0
147.0
215.0
316.0
Oct 2004
Jan 2005
Apr
Jul
Oct
Jan 2006
Apr
Jul
Oct
Jan 2007
Apr
Jul
Oct
Jan 2008
Apr
Jul
Oct
Jan 2009
Apr
Jul
16.5
12.0
7.5
3.0
-1.5
-6.0
-10.5
-15.0
Water / % deviation from mean

Figure 5

(a) 100 hPa

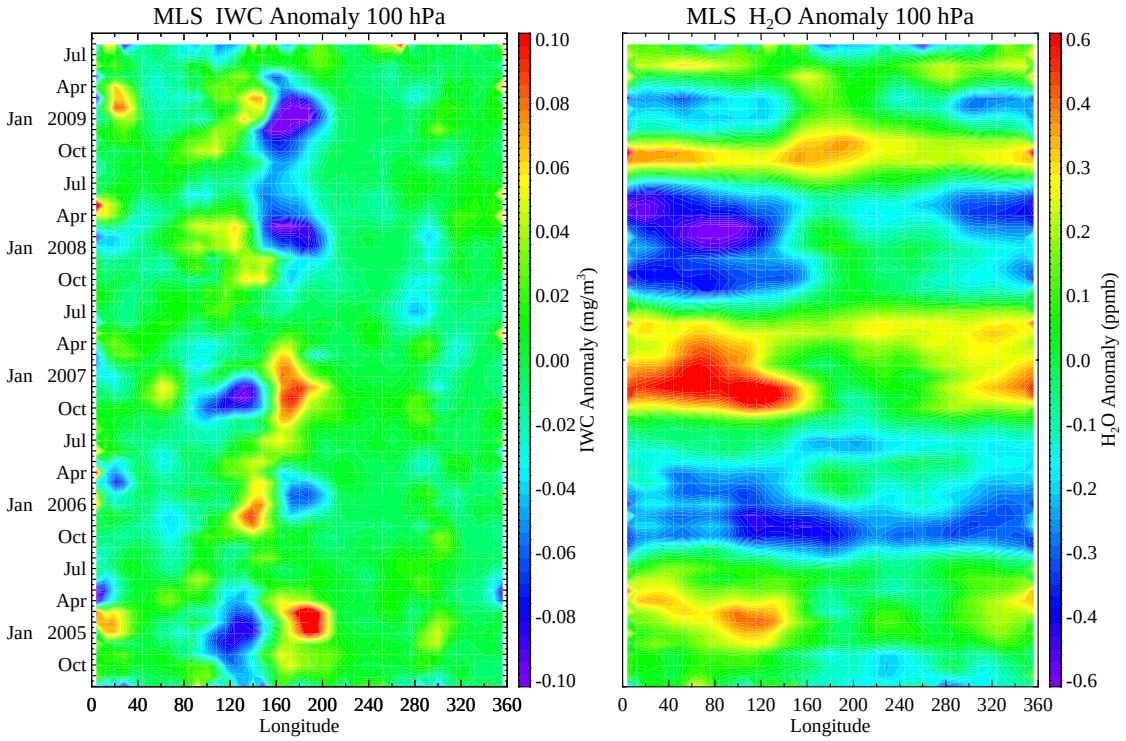

(b) 215 hPa

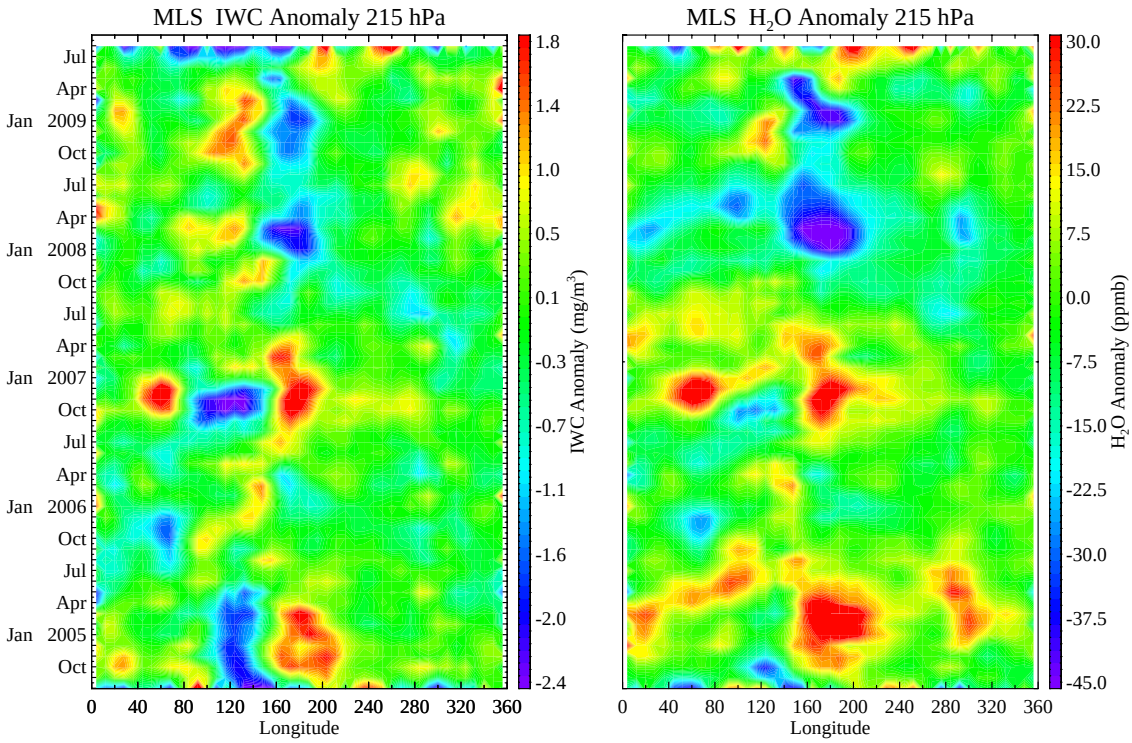

Figure 6

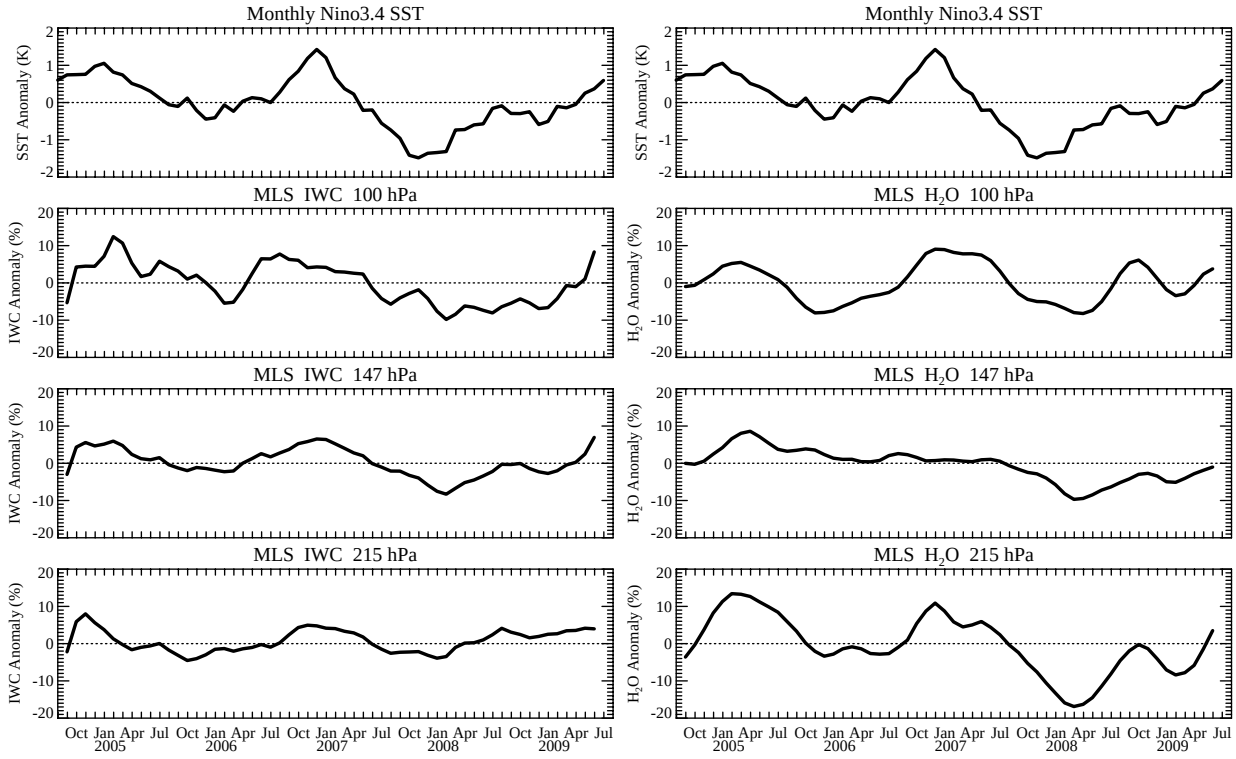
Monthly Nino3.4 SST
SST Anomaly (K)
MLS IWC 100 hPa
IWC Anomaly (%)
MLS H2O 100 hPa
H2O Anomaly (%)
MLS IWC 147 hPa
MLS H2O 147 hPa
MLS IWC 215 hPa
MLS H2O 215 hPa
Oct Jan Apr Jul Oct Jan Apr Jul Oct Jan Apr Jul Oct Jan Apr Jul Oct Jan Apr Jul
2005 2006 2007 2008 2009

Figure 7

(a) 2005 DJF Anomaly

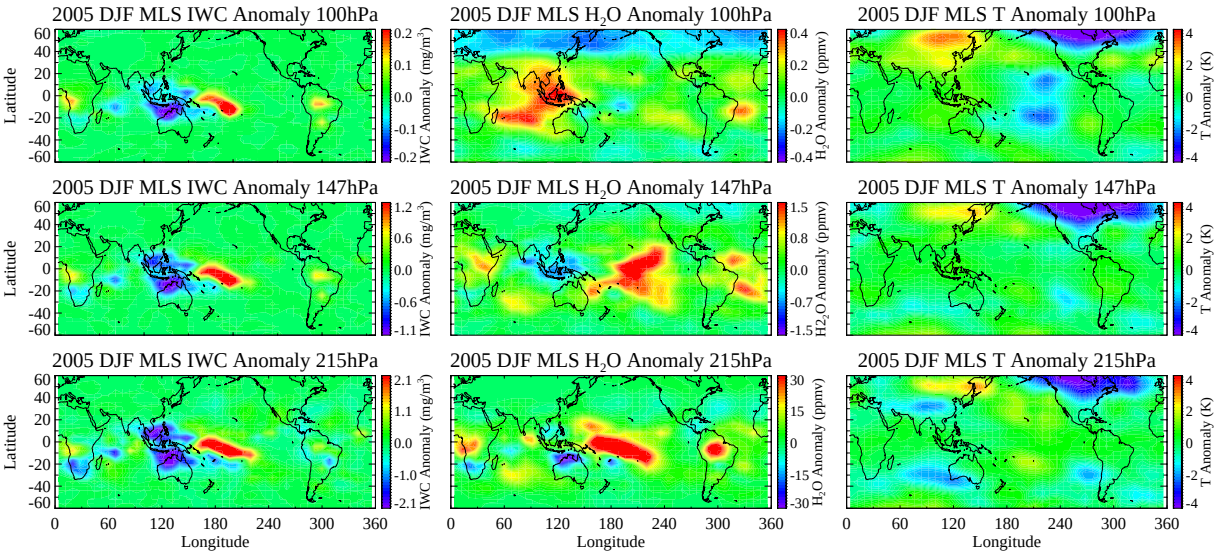

(b) 2008 DJF Anomaly

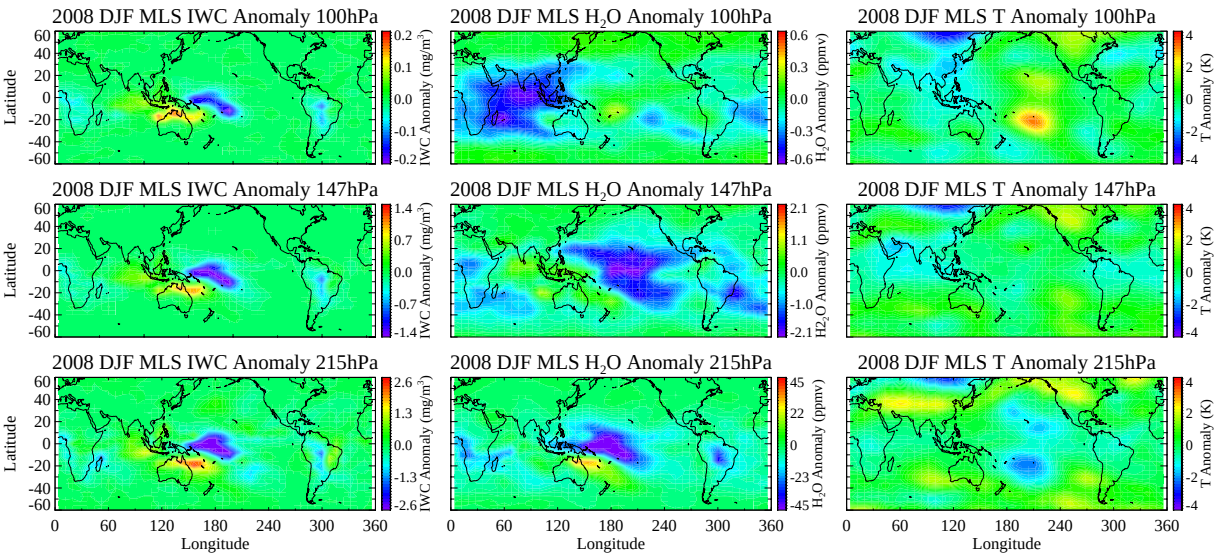

Figure 8

(a) GEOS-5 IWC

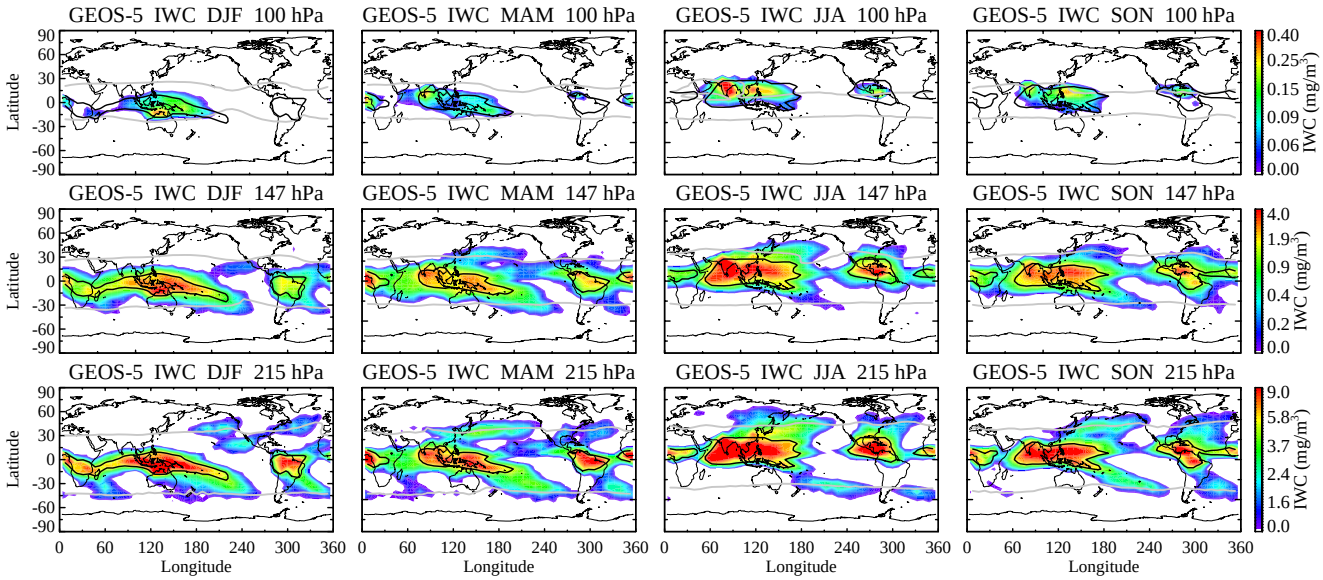

(b) GEOS-5 H_2O

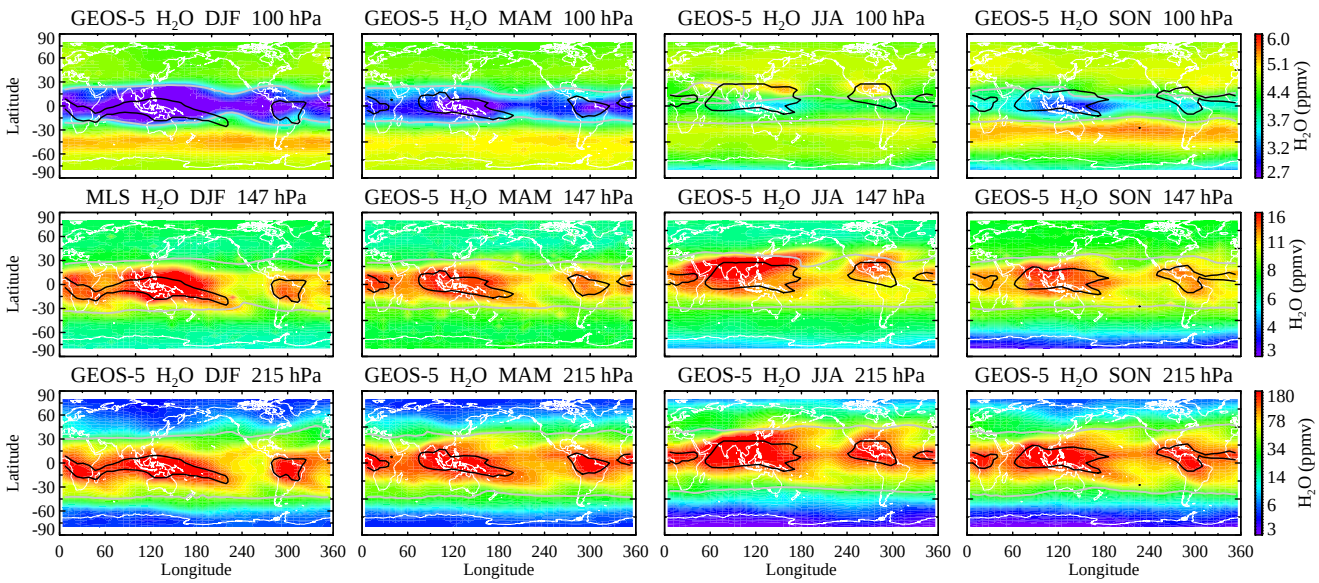

Supplementary Figure 1

(a) 100 hPa

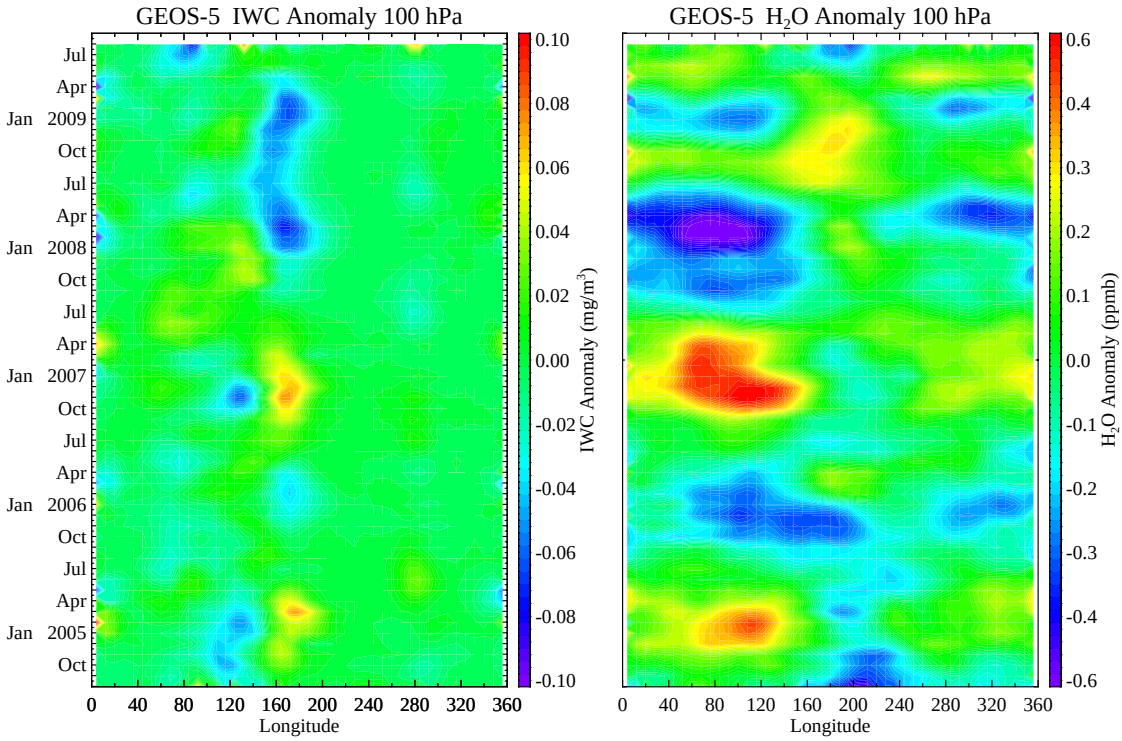

(b) 215 hPa

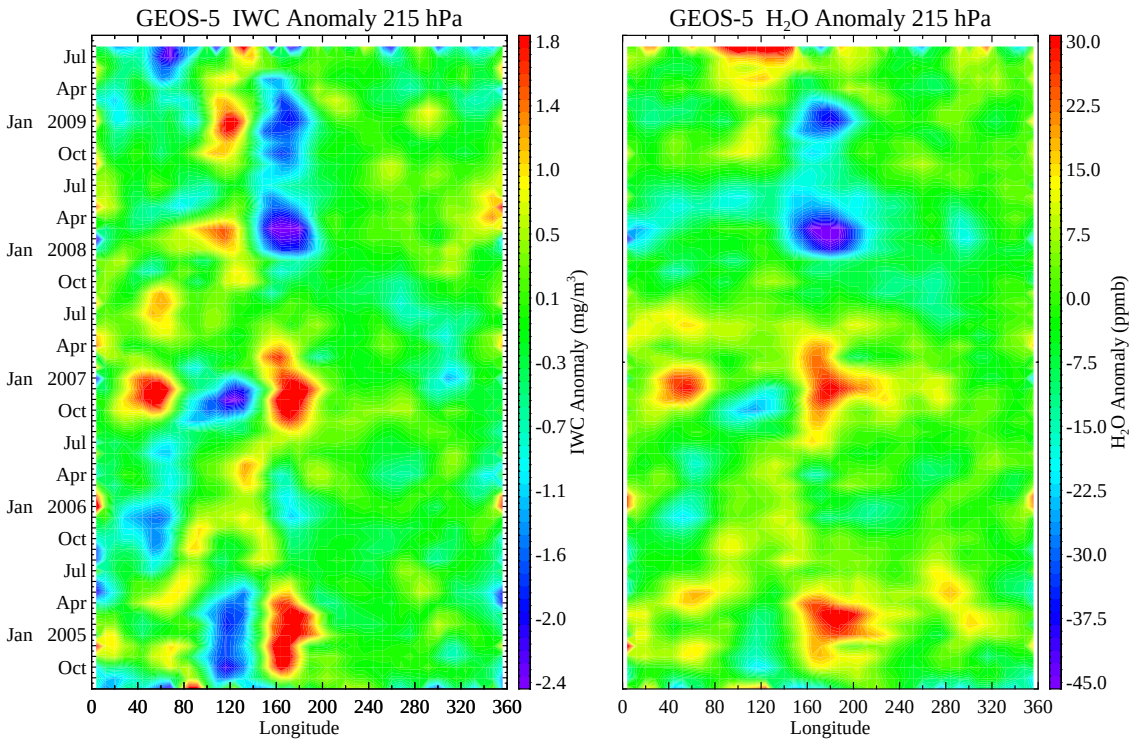

Supplementary Figure 2

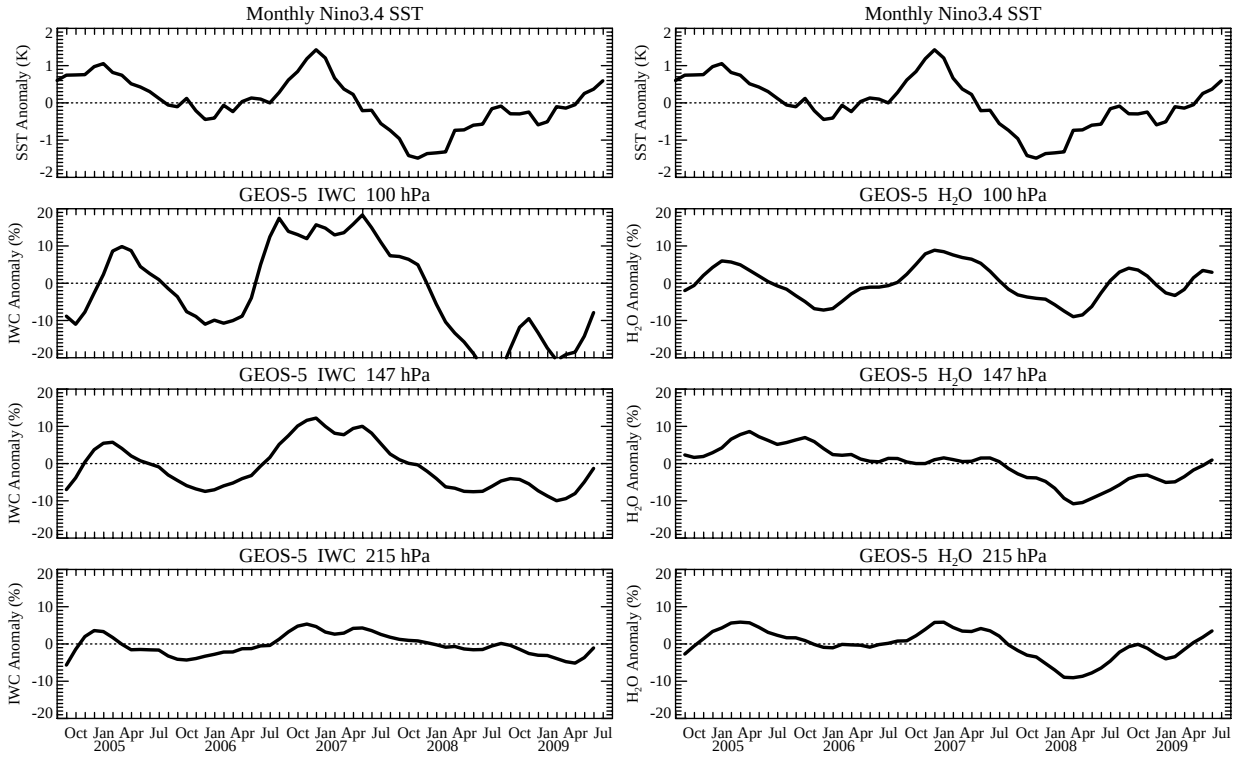

Supplementary Figure 3

(a) 2005 DJF Anomaly

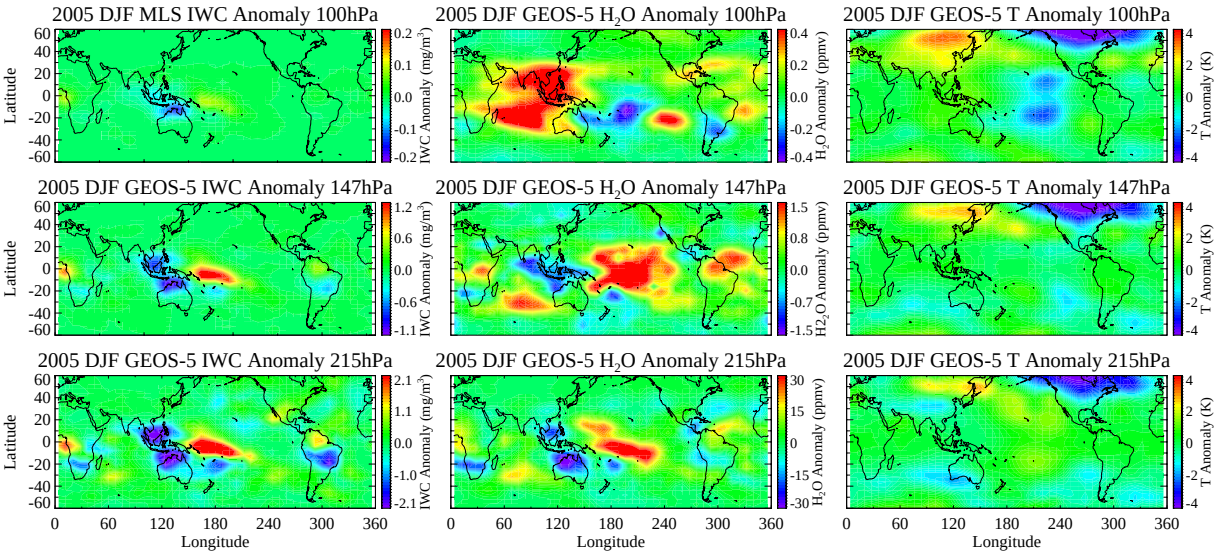

(b) 2008 DJF Anomaly

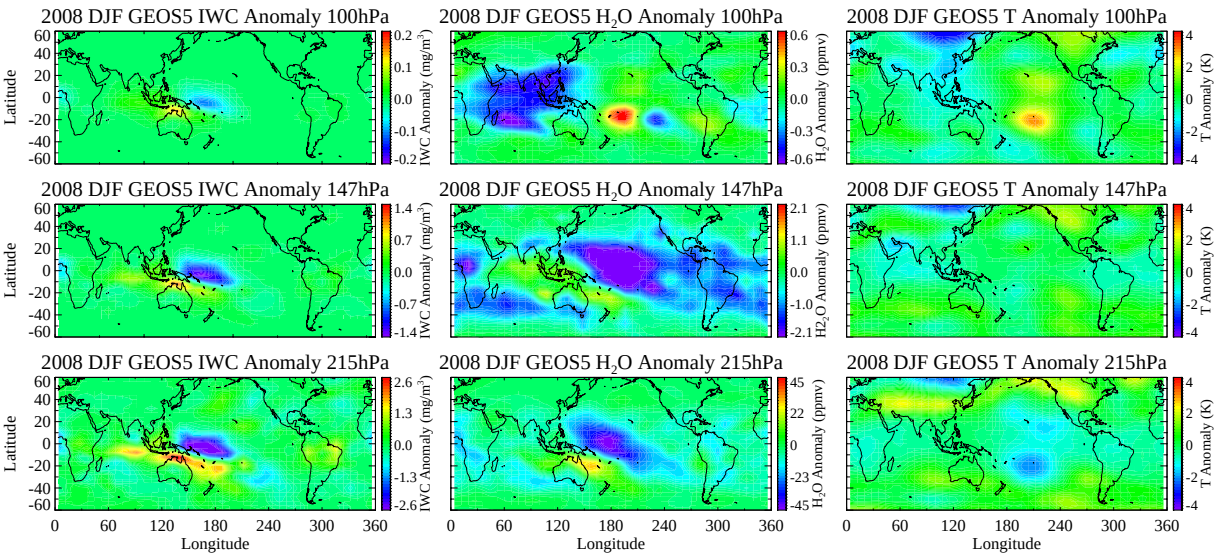

Supplementary Figure 4